# Oil & Natural Gas Technology

**DOE Award No.: DE-FE0013889**

**Quarterly Research Performance Progress Report (Period ending 12/31/2014)**

# THCM Coupled Model For Hydrate-Bearing Sediments: Data Analysis and Design of New Field Experiments (Marine and Permafrost Settings)

**Project Period (10/1/2013 to 09/30/2015)**

Submitted by:


Marcelo Sanchez Project PI

Texas A&M University
DUNS #: 847205572
College Station, TX
979-862-6604
msanchez@civil.tamu

J. Carlos Santamarina

Georgia Institute of Technology
Atlanta, Georgia
404-894-7605
edujcs@gatech.edu


Prepared for:
United States Department of Energy
National Energy Technology Laboratory
Submission date: 02/02/2015

**Office of Fossil Energy**

## DISCLAIMER

"This report was prepared as an account of work sponsored by an agency of the United States Government. Neither the United States Government nor any agency thereof, nor any of their employees, makes any warranty, express or implied, or assumes any legal liability or responsibility for the accuracy, completeness, or usefulness of any information, apparatus, product, or process disclosed, or represents that its use would not infringe privately owned rights. Reference herein to any specific commercial product, process, or service by trade name, trademark, manufacturer, or otherwise does not necessarily constitute or imply its endorsement, recommendation, or favoring by the United States Government or any agency thereof. The views and opinions of authors expressed herein do not necessarily state or reflect those of the United States Government or any agency thereof."

## ACCOMPLISHMENTS

*The experimental study of hydrate bearing sediments has been hindered by the very low solubility of methane in water (lab testing), and inherent sampling difficulties associated with depressurization and thermal changes during core extraction. This situation has prompted more decisive developments in numerical modeling in order to advance the current understanding of hydrate bearing sediments, and to investigate/optimize production strategies and implications. The goals of this research is to addresses the complex thermo-hydro-chemo-mechanical THCM coupled phenomena in hydrate-bearing sediments, using a truly coupled numerical model that incorporates sound and proven constitutive relations, satisfies fundamental conservation principles. This tool will allow us to better analyze available data and to further enhance our understanding of hydrate bearing sediments in view of future field experiments and the development of production technology.*

## ACCOMPLISHED

The project management plan (PMP, Task 1) and the selection of the PhD Students working during the 1st year of the project were competed and informed in the first quarterly report. The main accomplishments for this first period address Tasks 2, 3 and 4 of the original research plan, and include:

- Student training.
- Literature review.
- Update of constitutive equations.
- Update of THCM-Hydrate.
- Close-form analytical solutions.
- Numerical analyses

### Training

The training of the two PhD students working in this project has continued during this period. As for Mr. Xuerui (Gary) Gai (i.e. the Ph.D. student at TAMU), he is progressing in the understanding and modeling of problems involving has hydrate sediments. As for Mr. Zhonghao Sun (the Ph.D. student at GT), he has continued with the implementation of analytical solutions in MATLAB and other pieces of software. Both students have progressed positively with their coursework at their respective universities.

### Literature review

The literature review (Task 2) was completed during the previous periods.

### Update of Update of THCM-Hydrate

The updates of the constitutive laws for hydrate-bearing marine sediments and HBS in the permafrost (i.e. Task 3) were completed during the previous period.

### Close-form analytical solutions

The review on the main governing evolution laws, parameters, dimensionless ratios and simplifying assumptions for HBS dissociation has been continued during this period. A

study focus on the estimation of the maximum recoverable gas from hydrate bearing sediments is presented in this in this report (page 6).

**Numerical analyses**

The numerical analyses solving field production experiments as boundary value problems have been continued in this period.

**Plan - Next reporting period**

We will advance analytical and numerical fronts to enhance our code to solve coupled THCM problems involving with HBS, with renewed emphasis on simulating the natural processes under *in-situ* conditions and gas production.

Milestones for each budget period of the project are tabulated next. These milestones are selected to show progression towards project goals.

| | Milestone Title Planned Date and Verification Method | Actual Completion Date | Comments |
|---|---|---|---|
| Title<br>Related Task / Subtasks<br>Planned Date<br>Verification method | Complete literature review<br>2.0 / 2.a<br>March 2014<br>Report | March 2014 | Completed |
| Title<br>Related Task / Subtasks<br>Planned Date<br>Verification method | Complete updated Constitutive Equations<br>2.0 / 2.b & 2.c<br>June 2014<br>Report (with preliminary validation data) | July 2014 | Completed |
| Title<br>Related Task / Subtasks<br>Planned Date<br>Verification method | Validate new THCM constitutive equations<br>3.0 / 3.a, 3.b & 3.c<br>September 2014<br>Report (with first comparisons between experimental and numerical results) | September 2014 | Completed |
| Title<br>Related Task / Subtasks<br>Planned Date<br>Verification method | Complete close-form analytical solutions<br>4.0 / 4.a & 4.b<br>February 2015<br>Report (with analytical data) | February 2015 | Progressing as planned |
| Title<br>Related Task / Subtasks<br>Planned Date<br>Verification method | Complete numerical analyses<br>5.0 / 5.a, 5.b & 5.c<br>July 2015<br>Report (with analytical and numerical data) | July 2015 | Progressing as planned |
| Title<br>Related Task / Subtasks<br>Planned Date<br>Verification method | Complete THCM-Hydrate code modifications<br>6.0 / 6.a<br>June 2015<br>Report (with numerical data) | June 2015 | Progressing as planned |
| Title<br>Related Task / Subtasks<br>Planned Date<br>Verification method | Complete production optimization<br>7.0 / 7.a, 7.b, 7.c, 7.d & 7.e<br>September 2015<br>Report (with numerical data) | September 2015 | Progressing as planned |

## MAXIMUM RECOVERABLE GAS FROM HYDRATE BEARING SEDIMENTS (DEPRESSURIZATION)

### 1 Introduction

Natural gas hydrates are crystalline water and gas compounds. Stable thermodynamic conditions are met at high pressure and low temperature. Estimates of the global accumulation vary between $3x10^{15}$ $m^3$ and $10^{17}$ $m^3$ while the technically recoverable volume is on the order of $3x10^{14}$ $m^3$ (Sloan and Koh 2007; Boswell and Collett, 2011; Figure 1).

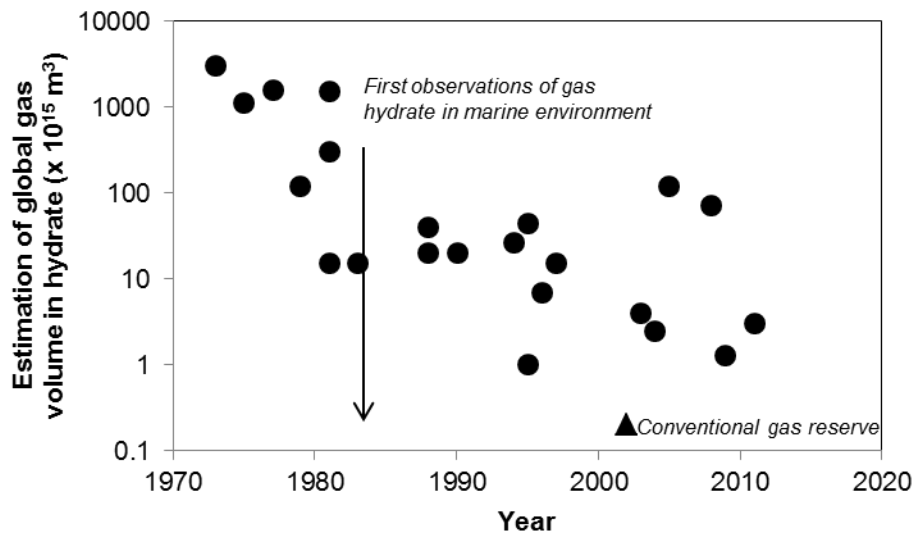


**Figure 1.** Estimation of global gas on the state of hydrate gas. From Sloan and Koh (2007); Boswell and Collett (2011). Notice conventional gas reserves are still orders of magnitude less than the worst of hydrate gas estimations.

Gas reservoirs in hydrate bearing sediments can be classified as (Moridis and Collett 2003; Moridis et al. 2011 and Moridis and Sloan 2007):

- **Class 1:** high hydrate saturation layer on top of a layer with free gas and water (i.e. Bottom Simulating Reflector BSR).
- **Class 2:** similar to class 1 but there is no free gas beneath (only mobile water).
- **Class 3:** absence of free fluids underneath (semi confined aquifer).
- **Class 4:** low hydrate saturation (< 10%), and lack of confining stratum.

Class 1 reservoirs are most desirable because they are next to the phase boundary and a low energy input is required for dissociation. Class 4 is least desirable because they lack confinement and can lead to very low recovery efficiency.

Sandy deposits are currently preferred because of their high permeability and low compressibility. Reservoirs that are considered to be commercially feasible given today's state of the art are listed in Table 1.

Table 1: Selected reservoirs gas volume estimation.

| **Location** | **Gas estimation [$m^3$]** | **Reference** |
|---|---|---|
| Mallik (Canada) | $3\ 10^9$ to $4\ 10^9$ | Moridis et al. 2002 |
| Gulf of Mexico | $6\ 10^{14}$ | BOEM report 2012 |
| Mount Elbert (Alaska) | $4\ 10^9$ | BOEM report 2012 |
| Atlantic coast USA | $6\ 10^{14}$ | BOEM report 2012 |
| Pacific coast USA | $2.3\ 10^{14}$ | BOEM report 2012 |
| Ulleung Basin (Korea) | $10^{15}$ to $10^{18}$ | Moridis et al. 2013 |
| Nankai Trough(Japan) | $5.6\ 10^{11}$ | Fujii et al 2013 |
| ShenhuArea (China) | $1.6\ 10^9$ | Wu et al. 2010 |
| Krishna-Godavari basin (India) | $9.8\ 10^8$ to $5.6\ 10^9$ | Shankar and Riedel 2011 |

*Note: the amount of gas in place, technically and economically recoverable is still under discussion, and its values change with respect to authors and computation methods (Figure 1).*

Methane gas can be produced from hydrate bearing sediments by (Moridis et al. 2008; Santamarina and Jang, 2009; Jang and Santamarina, 2011): (a) *depressurization*; (b) *thermal stimulation*; (c) *inhibitor's injection*, and (d) *$CO_2$-$CH_4$ replacement*. Several field tests have taken place as summarized in Table 2.

Table 2: Well tests summary in chronological order

| Name | Loc. | Year | Dur. | Type | Form. | $S_{hyd}$ [%] | Meas. $k_{eff}$ [mD] | Gas produced [$m^3$] | Affected radius [m] | Observ. | Reference |
|---|---|---|---|---|---|---|---|---|---|---|---|
| Mallik | Canada | 2002 | 123.7 hrs | Thermal stim. | Sand | 60 to 85 | 0.001 to 0.1 | 468 | 3 | Formation solids were produced | Hancock et al. (2005); Moridis et al. (2011) |
| Mt. Elbert | Alaska | 2007 | Several tests up to 13 hrs each | Depress. | Sand | 50 to 70 | 0.12 to 0.17 | $7\ 10^{-4}$ | 0.05 to 0.15 | | Boswell et al. (2008); Hunter et al. (2011); Anderson et al (2008) |
| Mallik | Canada | 2007 | 15hrs | Depress. | Sand | 60 to 85 | 0.1 to 1 | 830 | ND | Sand inflow causes operational problems | Dallimore et al. (2008) |
| | | 2008 | 6 days (139 hrs) | Depress. | | | ND | 13000 | ND | | Yamamoto and Dallimore (2008) |
| Nankai Trough | Japan | 2013 | 6 days | Depress. | Layd. | ND | ND | 120000 | ND | First offshore production - | www.jogmec.go.jp |

mD = $10^{-12}$ $m^2$
ND = No data provided

The analysis of gas production requires complex coupled thermo-hydro-mechanical codes such as (Moridis et al. 2014; Hong and Pooladi-Darvish 2005; Moridis et al. 2008; Walsh et al. 2009; Konno et al. 2010; Pruess 2003; CMG 2012; Nagao 2011): TOUGH + HYDRATE (Lawrence National Lab), MH21-HYDRES (Japan Oil Engineering Company), CMG-STARS (Computer Modelling Group, Canada), STOMP-HYD (Pacific Northwest National Laboratory). These codes involve a large number of equations, constitutive relations and parameters. They are complex and suffer from time- and space-discretization errors (Pooladi-Darvish 2004). Table 3 shows some of the key parameters involved in these simulations.

Analytical solutions have been proposed to analyze local conditions (Kwon et al. 2008) thermal stimulation (Ullerich et al. 1987; Esmaeilzadeh et al. 2011; Klar et al., 2013), and depressurization (Goel et al, 2001; Ji et al., 2001; Hong et al. 2003; Tsypkin 2000). However these analyses remain complex, require iterative solution and hide explicit relations between governing parameters.

The pressure distribution in radial flow is inversely proportional to the logarithm of the radial distance to the well. Therefore there is a physical limit to the zone around a well that can experience pressure-driven dissociation. The study reported herein was conducted to develop a simple and robust set of equations to estimate limits for gas production from hydrate bearing sediments using depressurization.

Table 3: Summary of selected parameters used in numerical simulations

| **Well rad. [m]** | **Dom. radius [m]** | **Hyd. thick. [m]** | **Initial press. [MPa]** | **Well press. [MPa]** | **Initial temp. [K]** | **Intrinsic Perm. [$m^2$ or mD]** | **Porosity [--]** | **Reference** |
|---|---|---|---|---|---|---|---|---|
| 0.1 | 10000 | 1 | 5.7 | 2.7 | 278.85 | $1\ 10^{-15}$ to $1\ 10^{-12}$ $m^2$ | 0.30 to 0.60 | Moridis and Sloan (2007) |
| ND | 567.5 | 15 | 10 | ND | 286.65 | $1\ 10^{-12}$ $m^2$ | 0.3 | Moridis and Kowalsky (2006) |
| 0.1 | 45 | 23 | 13 | 2.93 | 274.2 | $1\ 10^{-15}$ $m^2$ | 0.3 | Li et al (2012) |
| ND | ND | 20, 16, 10 | 10.8, 9, 10.8 | ND | 285 | $2\ 10^{-14}$ $m^2$ | 0.28 | Moridis et al (2002) |
| 0.1 | 450 to 1500 | 200 | (Varies) | 2.7 | ND | 1000 mD | 0.3 to 0.64 | Myshakin et al (2012) |
| 0.1 | 100 | 10 | 11.5 | 3, 4 and 5 | 287.15 | $1\ 10^{-14}$ $m^2$ | 0.38 | Su et al (2012) |
| 0.1 | 400 | 11.3 | 6.4 | 3 | 275.5 | $1\ 10^{-12}$ $m^2$ | 0.4 | Moridis et al (2011) |
| 0.1 | 250 | 20 | 23 | 3 | 289 | $5\ 10^{-13}$ $m^2$ (**) | 0.45 to 0.65 | Moridis et al (2013) |
| ND | 120 | 70, 100 | 13, 8.7, 13 | 3 | 287 | 1000 to 0.1 mD | 0.3 to 0.4 (***) | Kurihara et al (2009) |
| 0.1 | 45 | 22 | 13.8 | 0.2 Po | 287 | $7.5\ 10^{-14}$ $m^2$ | 0.41 | Li et al (2010) |
| 0.1 | 250 | 50 | 6.7 to 12.13 | 4 | 282 to 287 | 10 to 500 mD | 0.4 | Konno et al (2010) |

(*) computed from model proposed by Stone (1970) $_{rA} = (S^*_A)^n$; $S^*_A = (S_A - S_{irA})/(1-S_{irA})$; $k_{rG} = (S^*_G)^n$; $S^*_G = (S_G - S_{irG})/(1-S_{irG})$

(**) estimated value

(***) varies for clay, silt and sand

(****) For the case of Class 3: 14° C and ko = 500mD

ND = no data provided

Table 3: Summary of selected parameters used in numerical simulations (cont.)

| | Relative permeability (*) | | | | |
|---|---|---|---|---|---|
| | | Water | Gas | | |
| **Hydrate saturation [--]** | **n [--]** | **$S_{irA}$ [--]** | **$S_{irG}$ [--]** | **Observations** | **Reference** |
| 0.02 to 0.1 | 4 | 0.2 | 0.02 | Parametric study –Dissoc. pressure is computed by the software | Moridis and Sloan (2007) |
| 0.7 | 3 | 0.25 | 0.02 | Class 1 and 2 hydrate deposit studied | Moridis and Kowalsky (2006) |
| 0.4 | 3.57 | 0.25 | 0.05 | Simulating Qilian Mountain Permafrost - China | Li et al (2012) |
| 0.8, 0.5, 0.8 | 4.2 | 0.2 | 0.05 | Simulating different zones @ Mallik reservoir - Canada - vertical and horizontal wells | Moridis et al (2002) |
| 0.05 to 0.80 | 3.16 | 0.18 | 0.02 | Simulating layered sediments in Gulf of Mexico Walker Ridge 313 site | Myshakin et al (2012) |
| 0.1, 0.2 and 0.3 | 5 | 0.3 | 0.03 | Parametric study of Shenhu Area China | Su et al (2012) |
| 0.65 | 4.2 | 0.2 | 0.02 | Parametric study of Mount Albert, Alaska | Moridis et al (2011) |
| 0.3 to 0.7 | 3.5 | 0.2 | 0.01 | Simulating layered sediments Ulleung Basin, Korea | Moridis et al (2013) |
| 0.1 to 0.96 | ND | ND | ND | Layered system of sand, silt and clay of Nankai Trough, Japan | Kurihara et al (2009) |
| 0.44 | 3.57 | 0.3 | 0.05 | Sea of south of China, Shenhu | Li et al (2010) |
| 0.6 | $k = ko\ (1\text{-}Sh)^2$ | | | Class 1, 2 and 3 reservoirs | Konno et al (2010) |

(*) computed from model proposed by Stone (1970) $_{rA} = (S^*_A)^n$; $S^*_A = (S_A - S_{irA})/(1\text{-}S_{irA})$; $k_{rG} = (S^*_G)^n$; $S^*_G = (S_G - S_{irG})/(1\text{-}S_{irG})$

(**) estimated value

(***) varies for clay, silt and sand

(****) For the case of Class 3: 14° C and ko = 500mD

ND = no data provided

## 2 Analytical Solution

Consider a gas hydrate reservoir in a host sediment under high water pressure and low temperature. Gas production starts as soon as the decreasing pressure brings the hydrate outside stability conditions. The host sediment will experience: permeability changes, settlement, fines migration, unsaturation and gas expansion (Jang and Santamarina, 2011).

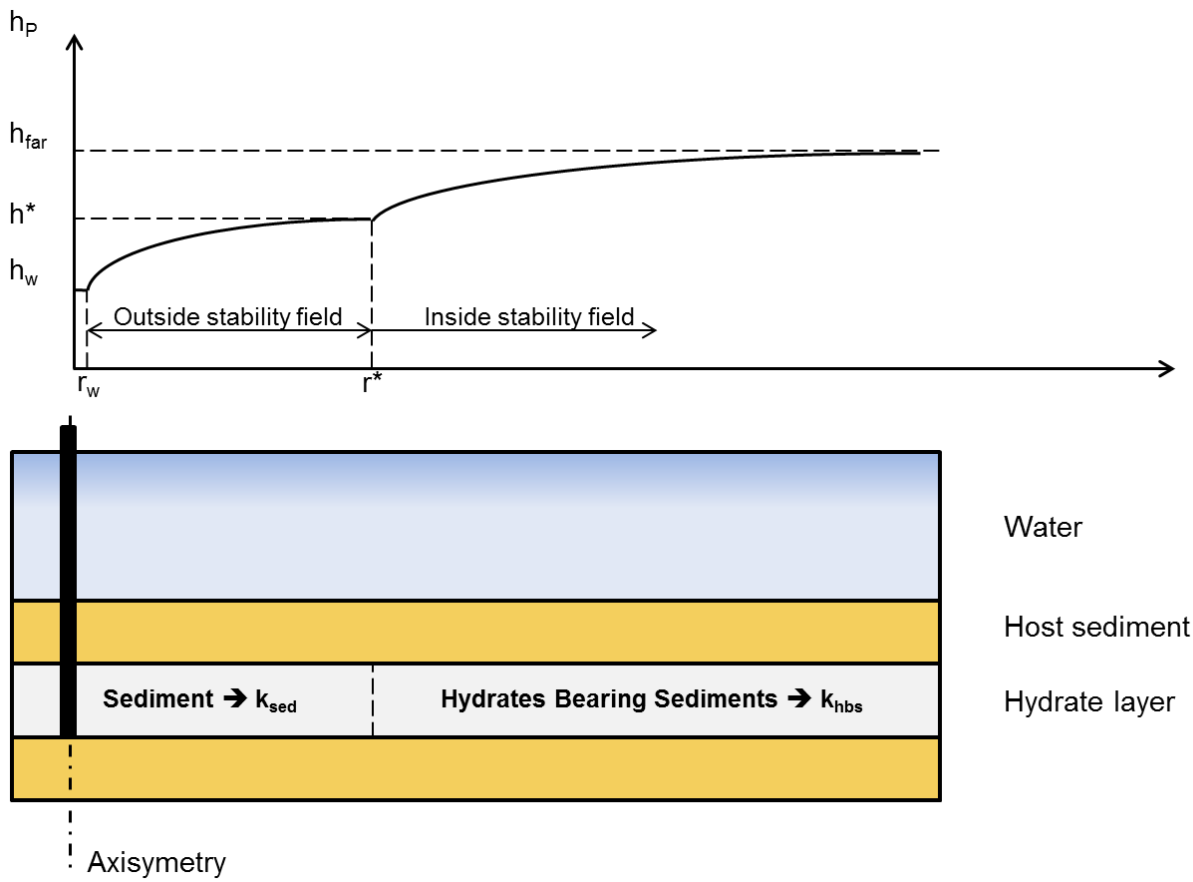


**Figure 2.** General description of the problem. Below the seafloor, a hydrate layer is located immersed in a generic host sediment. As soon as the production pipe decreases the pressure to $h_w$, two zones can be defined. The first one from the well to the dissociation front and beyond the dissociation front; both with different permeability values.
Note: sub-indices: w = well; far = far field; * = dissociation front

Two zones can be identified under steady state conditions when the pressure drop is kept constant and hydrate stops dissociating (Figure 2): the inner zone where hydrate

has been depleted, and the outer zone where hydrate remains stable. Let's define the size of the produced zone as r* [m], and the total head pressure in the far field as $h_{far}$ [m]. The inner zone is characterized by the permeability of the sediment without hydrates ($k_{sed}$) and the outer zone by the permeability of the hydrate bearing sediment ($k_{hbs}$). Clearly, gas was produced from the inner zone $r \leq r^*$.

### 2.1 Thin or Deep Reservoir Condition

The pressure field around a production well when continuity and Darcian conditions are satisfied is defined by Laplace's equation, in terms of the total energy $E_{tot}$, or of the total head $h_t = E_{tot}/mg$, where mg define the fluid unit weight; then, in cartitian coordinates:

$$\nabla E_{tot} = \nabla^2 h_t = 0 \tag{1}$$

However, stability conditions and the dissociation front are determined by the pore water pressure $u = (h_t – h_e)\ \gamma_w$, where u is the pore pressure, $h_e$ elevation pressure. In most cases, the thickness of the hydrate bearing sediment layer is much smaller than the depth at which the hydrate layer is located or depressurization is much greater than the affected geometry $\Delta u >> \Delta h_e$. Then we can assume that the effect of elevation on total head is negligible, and we link total head $h_t$ directly to pressure head $u = h_t$. Then fluid pressure becomes $u = h_t\ \gamma_w$. Spherical and axisymmetric flow conditions are analyzed next.

### 2.2 Homogeneous Formation: Spherical Flow Condition

<u>*Radial flow*</u>. Laplace's equation in spherical coordinates is (Figure 3):

$$\nabla^2 h = \frac{1}{r^2}\frac{\partial}{\partial r}\left(r^2\ \frac{\partial h}{\partial r}\right) + \frac{1}{r^2\ sin(\theta)}\frac{\partial}{\partial \theta}\left(sin(\theta)\ \frac{\partial h}{\partial \theta}\right) + \frac{1}{r^2\ sin^2(\theta)}\frac{\partial^2 h}{\partial \xi^2} = 0 \tag{2}$$

where the azimuthal angle θ, the polar angle ξ and the radius r define the location of any point on a sphere.

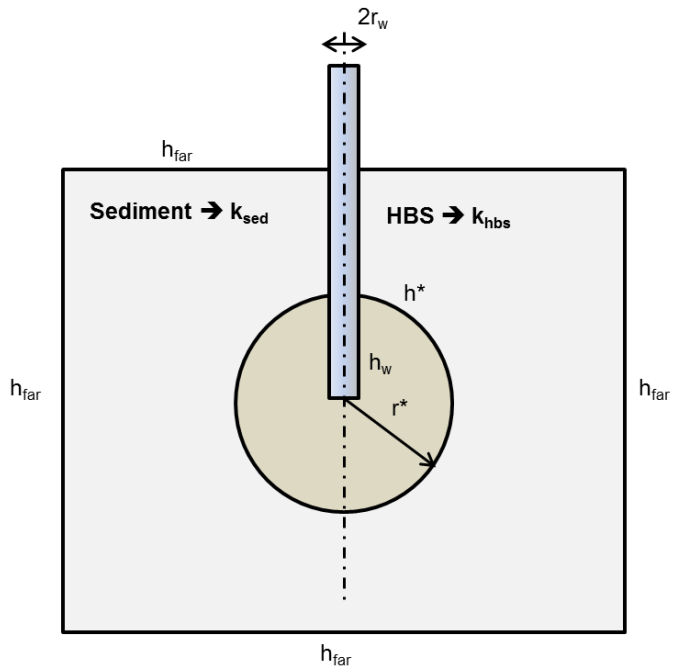


**Figure 3.** General description for the spherical dissociation front case.

Radial flow tangential derivatives are zero and the equation simplifies to:

$$\nabla^2 h = \frac{1}{r^2}\frac{\partial}{\partial r}\left(r^2\,\frac{\partial h}{\partial r}\right) = 0 \tag{3}$$

Which means:

$$r^2\,\frac{\partial h}{\partial r} = constant = C_1 \tag{4}$$

Hence:

$$h = -\frac{C_1}{r} + C_2 \tag{5}$$

Let's select the following boundary conditions:

$$\begin{aligned} &\text{At the well: } h = h_w : \quad r = r_w \\ &\text{At far field: } h = h_{far} : \quad r = r_{far} \end{aligned} \tag{6}$$

Where $r_w$ [m] is the well radius and $r_{far}$ [m] is the radius of influence of the well. Then:

$$h_w = -\frac{C_1}{r_w} + C_2 \qquad and \qquad h_{far} = -\frac{C_1}{r_{far}} + C_2 \tag{7}$$

which gives us:

$$h = \frac{h_{far} - h_w}{\frac{1}{r_{far}} - \frac{1}{r_w}} \left( \frac{1}{r} - \frac{1}{r_w} \right) + h_w \tag{8}$$

The velocity can be computed from Darcy's law:

$$v_r = -k \frac{\partial h}{\partial r} = k \frac{h_{far} - h_w}{\frac{1}{r_{far}} - \frac{1}{r_w}} \frac{1}{r^2} \tag{9}$$

where k [m/sec] is the permeability. The flow rate q [$m^3$/sec] becomes:

$$q = -k \int_0^{2\pi} d\xi \int_0^{\pi} r^2 v_r \, sin(\theta) d\theta \tag{10}$$

If the total head is known at two radial distances $r_1$ and $r_2$, then the flow rate is:

$$q = k \frac{4\pi (h_2 - h_1)}{\frac{1}{r_1} - \frac{1}{r_2}} \tag{11}$$

<u>*Dissociation Boundary r*.*</u> At state conditions, the dissociation front stops expanding at the terminal position r*, there is no more dissociation, and water flow rate continuity is satisfied at the boundary between the inner hydrate-free sediment and outer hydrate bearing medium. Hence:

$$q_{sed} = q_{hbs} \tag{12}$$

$$\frac{(h^* - h_w) k_{sed}}{\frac{1}{r_w} - \frac{1}{r^*}} = \frac{(h_{far} - h^*) k_{hbs}}{\frac{1}{r^*} - \frac{1}{r_{far}}} \tag{13}$$

Since $1/r_{far} \rightarrow 0$, this equation predicts that the size of the dissociation front r* can be estimated as (Figure 4):

$$r^* = r_w \left( 1 + \frac{k_{sed}}{k_{hbs}} \frac{h^* - h_w}{h_{far} - h^*} \right) \tag{14}$$

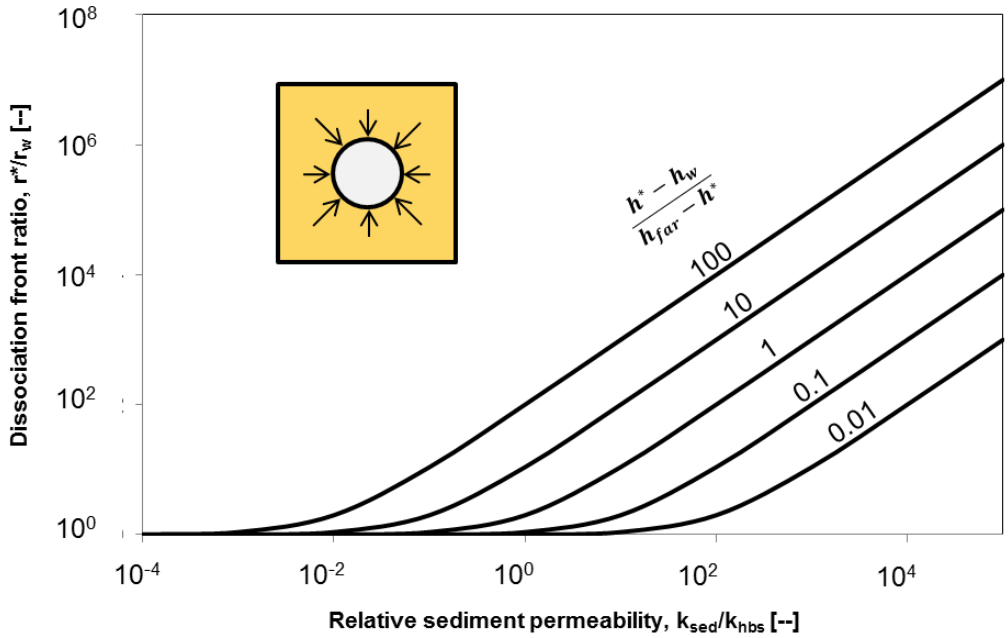


**Figure 4.** Spherical dissociation front. Relationship between dissociation radius, permeabilities and pressure.

### 2.3 Layered Formation: Axisymmetric Flow with Leak-in Condition

Consider a hydrate bearing sandy reservoir confined between two low permeability layers (Figure 5-a).

The conservation of mass in this annulus is:

$$q_r = q_{r+dr} + \Delta q \tag{15}$$

$$V_r\, 2\pi r H = V_{r+dr} 2\pi (r+dr) H + \pi[(r+dr)^2 - r^2] V^+ \tag{16}$$

where $V^+$ [m/sec] is the velocity perpendicular to the horizontal plane. Once again, this equation is in terms of $h_t$, however we consider small changes in elevation so that $h_t \approx u$. Applying Darcy's law:

$$k \left.\frac{\partial h}{\partial r}\right|_r 2rH = k \left.\frac{\partial h}{\partial r}\right|_{r+dr} 2(r+dr)H + 2\, r\, dr k' \frac{h^+ - h}{b} \tag{17}$$

where h is the total head at any point evaluated at a determined distance, k' [m/s] is the aquitar permeability, b [m] the aquitard layer thickness and $h^+$ is the total head outside

the semi-confined aquifer.

$$\frac{\left.\frac{\partial h}{\partial r}\right|_{r} - \left.\frac{\partial h}{\partial r}\right|_{r+dr}}{dr}\, rH = \left.\frac{\partial h}{\partial r}\right|_{r+dr} H + r\,\frac{k'}{k}\,\frac{h^{+} - h}{b} \tag{18}$$

$$\frac{\partial^2 h}{\partial r^2} = \frac{1}{r}\,\frac{\partial h}{\partial r} + \frac{k'}{k}\,\frac{h^{+} - h}{Hb} \tag{19}$$

The solution of this equation is (De Glee 1951):

$$q = \frac{2\,\pi\,k\,H}{K_0\left(\frac{r}{\sqrt{\frac{k\,H\,b}{k'}}}\right)} \tag{20}$$

where $K_o$ is the modified hyperbolic Bessel function of the second kind and order zero.

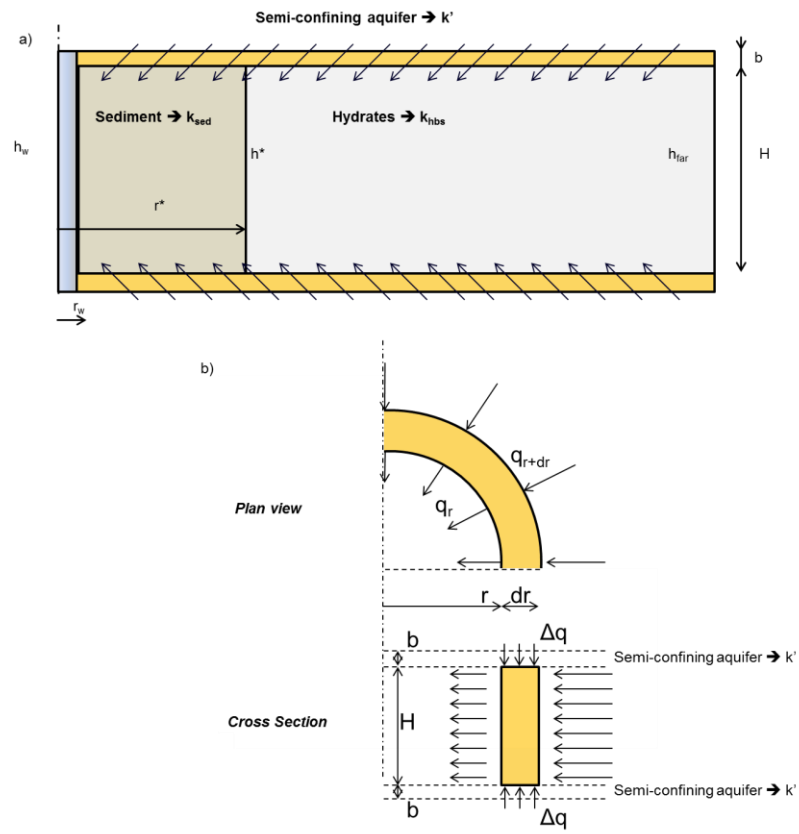


**Figure 5:** Leaky aquifer case. a) General description, where H = hydrate layer thickness, $k_{sed}$ = sediment permeability, $k_{hyd}$ = hydrate layer permeability, $h_w$ = well water pressure, h* = dissociation pressure, $h_{far}$ = far field water pressure, r* = dissociation front, $r_w$ = well radius. b = aquitard thickness, k' = aquitard permeability. (b) General description for the double semi-confined aquifer.

For steady state conditions, the water flow rates at the boundary between the hydrate free inner zone and outer hydrate bearing sediment zones satisfy mass conservation:

$$q_{sed} = q_{hbs} \tag{21}$$

$$\frac{k_{sed}\,(h^* - h_w)}{K_0\left(\frac{r_w}{\sqrt{\frac{k_{sed}\,H\,b}{k'}}}\right)} = \frac{k_{hbs}\,(h_{far} - h^*)}{K_0\left(\frac{r^*}{\sqrt{\frac{k_{hbs}\,H\,b}{k'}}}\right)} \tag{22}$$

$$\frac{k_{sed}}{k_{hbs}}\,\frac{h^* - h_w}{h_{far} - h^*} = \frac{K_0\left(\sqrt{\frac{k'}{k_{sed}}\,\frac{r_w^2}{H\,b}}\right)}{K_0\left(\sqrt{\frac{k'}{k_{hbs}}\,\frac{r^{*2}}{H\,b}}\right)} \tag{23}$$

Different approximations to Bessel functions are identified for different ranges of the argument. Figure 6 shows the hyperbolic Besssel function of the second kind and order zero, and two different approximations: a logarithmic function fits best for the argument < 0.5, while the exponential fits best for 0.3 <argument< 7.

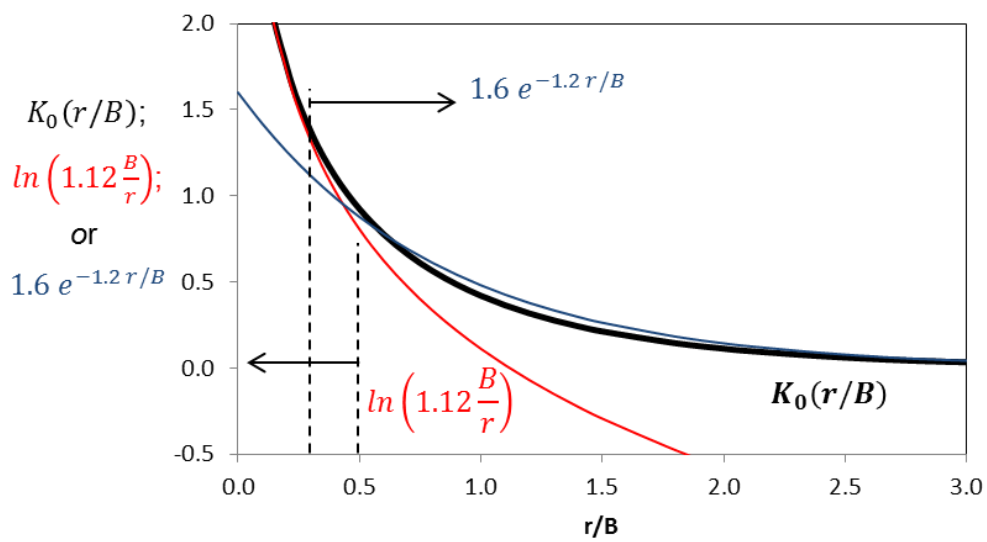


**Figure 6.** Leaky aquifer case. Best fit for Bessel equation (Ko) for r/B < 0.5 and r/B > 0.3.

Note: B = $\sqrt{\frac{k\,H\,b}{k'}}$

Then the following explicit equations apply to different scenarios:

*Case A:* $\sqrt{\frac{k'}{k_{sed}}\frac{r_w^2}{H\ b}} < 0.5$ and $\sqrt{\frac{k'}{k_{hbs}}\frac{r^{*2}}{H\ b}} < 0.5$

$$\frac{k_{sed}}{k_{hbs}}\frac{h^* - h_w}{h_{far} - h^*} = \frac{Ln\left(1.12\sqrt{\frac{k_{sed}\ H\ b}{k' r_w^2}}\right)}{Ln\left(\frac{1.12\sqrt{\frac{k_{hbs}\ H\ b}{k'}}}{r^*}\right)} \tag{24}$$

$$\frac{r^*}{r_w} = \frac{1.12\sqrt{\frac{k_{hbs}}{k'}\frac{H\ b}{r_w^2}}}{\left(1.12\sqrt{\frac{k_{sed}}{k'}\frac{H\ b}{r_w^2}}\right)^{\left(\frac{k_{sed}}{k_{hbs}}\frac{h^* - h_w}{h_{far} - h^*}\right)^{-1}}} \tag{25}$$

*Case B:* $\sqrt{\frac{k'}{k_{sed}}\frac{r_w^2}{H\ b}} > 0.3$ and $\sqrt{\frac{k'}{k_{hbs}}\frac{r^{*2}}{H\ b}} > 0.3$

$$\frac{k_{sed}}{k_{hbs}}\frac{h^* - h_w}{h_{far} - h^*} = \frac{1.6\ e^{\left(-1.2\ r_w \Big/ \sqrt{\frac{k_{sed}\ H\ b}{k'}}\right)}}{1.6\ e^{\left(-1.2\ r^* \Big/ \sqrt{\frac{k_{hbs}\ H\ b}{k'}}\right)}} \tag{26}$$

$$\frac{r^*}{r_w} = \sqrt{\frac{k_{hbs}}{k_{sed}}}\left[1 + \frac{1}{1.2}\sqrt{\frac{k_{sed}}{k'}\frac{H\ b}{r_w^2}}\ Ln\left(\frac{k_{sed}}{k_{hbs}}\frac{h^* - h_w}{h_{far} - h^*}\right)\right] \tag{27}$$

*Case C:* $\sqrt{\frac{k'}{k_{sed}}\frac{r_w^2}{H\ b}} < 0.5$ and $\sqrt{\frac{k'}{k_{hbs}}\frac{r^{*2}}{H\ b}} > 0.3$

$$\frac{k_{sed}}{k_{hbs}}\frac{h^* - h_w}{h_{far} - h^*} = \frac{Ln\left(1.12\sqrt{\frac{k_{sed}\,H\,b}{k' r_w^2}}\right)}{1.6\,e^{\left(-1.2\Big/\sqrt{\frac{k_{hbs}\,H\,b}{k' r^{*2}}}\right)}} \tag{28}$$

$$\frac{r^*}{r_w} = \frac{1}{1.2}\sqrt{\frac{k_{hbs}}{k'}\frac{H\,b}{r_w^2}}\;Ln\left[\frac{1.6\,\frac{k_{sed}}{k_{hbs}}\,\frac{h^* - h_w}{h_{far} - h^*}}{Ln\left(1.2\sqrt{\frac{k_{sed}}{k'}\frac{H\,b}{r_w^2}}\right)}\right] \tag{29}$$

## 3 Discussion

The spherical is the simplest case, in which the relative sediment permeability $k_{sed}/k_{hbs}$ and relative pressure dissociation control the dissociation front. Near the phase boundary ($h_{far} - h^*$) → 0 and sediments with high hydrate saturation so that $k_{sed} >> k_{hbs}$ lead to larger production zones r*. The critical role of the "effective well radius" $r_w$ is also highlighted.

For the leaky aquifer case scenario, the equations are defined with 10 variables controls the dissociation front: dissociation radius r*, well effective radius $r_w$, hydrate layer thickness H, aquitard thickness b, hydrate bearing sediment permeability $k_{hbs}$, aquitard permeability k', sediment permeability $k_{sed}$, dissociation pressure h*, well pressure $h_w$ and far field pressure $h_{far}$. Nevertheless, only two units are involved: [L] and [T], which means that there are 8 possible dimensionless ratios (Buckingham's theorem). The equations for all cases already show important dimensionless ratios as: relative sediment permeability $k_{sed}/k_{hbs}$, relative leak-in permeability $k_{sed}/k'$, relative pressure dissociation $(h^* - h_w)/(h_{far} - h^*)$ and a geometrical ratio $H\,b/r_w^2$. The comments for the spherical case also apply for the leak-in condition. The geometrical ratio represents the importance of the leaky aquifer respect to the hydrate bearing sediment layer, as H increases the pro-

duction zone.

**4 Recoverable Gas: Energy**

The energy density of gas methane is $E_d$ = 46 MJ/kg STP, while the density for hydrate is just $E_d$ = 4.8 MJ/kg of hydrate mass (Hermann, 2005). The recoverable energy RE [J] from a hydrate bearing sediment with hydrate saturation $S_{hyd}$ [--] when V [$m^3$] is:

$$RE = V\ n\ S_{hyd}\ E_d\ \rho_{hyd}\ e \tag{30}$$

where n is the porosity, and e the gas recovery efficiency. The recovery efficiency e depends on the interaction of gas with other fluids (such as water) in the reservoir as a function of pore size distribution and connectivity (Jang and Santamarina 2011). For the case when gas is the only fluid displaced and water remains in the reservoir (represents the case with maximum gas recovery).

$$e = \frac{\beta - 1}{\beta - 0.79} \tag{31}$$

where β is the fluid expansion factor as the ratio of the combined gas and water volumes to the initial volume of hydrate. Typical values are β = 1.3 (u = 30 MPa) and e = 0.6; and β = 6 (u = 3 MPa) and e = 0.96. Figure 7 shows the profit per hydrate thickness vs. radius of dissociation r* estimated for selected reservoirs. The most profitable extraction reservoirs are the Ulleung Basin and Nankai Trough where the cost of gas is almost 4 times the price in USA (FERC: Federal Energy Regulatory Commission - www.ferc.gov). The low costs of gas extraction in USA hinder the possibility of gas extraction in the near future. Table 4 summarizes values used for these computations.

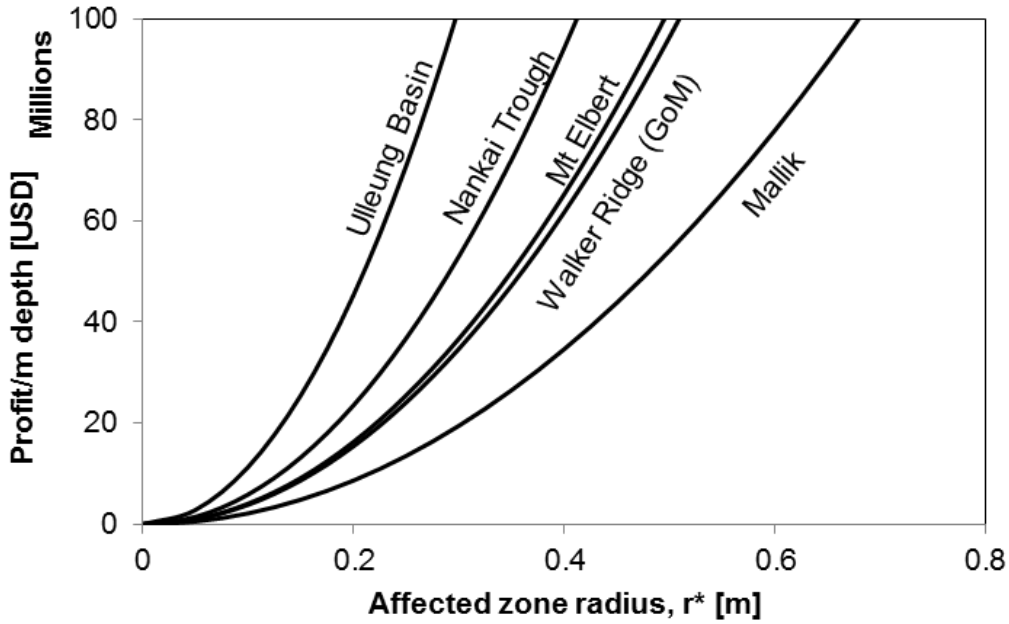


**Figure 7.** Economical analysis. Profit per hydrate thickness with respect to dissociation front for selected potential locations.

Table 4: Profit analysis

| | | Reservoir | | | | |
|---|---|---|---|---|---|---|
| **Parameter** | **Unit** | **Mallik** | **Walker Ridge (GoM)** | **Mt El-bert** | **Korea** | **Japan** |
| $H_{hyd}$ | [m] | 10 | 200 | 11 | 20 | 100 |
| $k_{sed}$ | [m/s] | $10^{-7}$ | $10^{-7}$ | $10^{-6}$ | $10^{-6}$ | $10^{-7}$ |
| $k_{hbs}$ | [m/s] | $10^{-9}$ | $10^{-8}$ | $10^{-9}$ | $10^{-9}$ | $10^{-8}$ |
| n | [--] | 0.28 | 0.5 | 0.4 | 0.5 | 0.35 |
| $S_{hyd}$ | [--] | 0.5 | 0.7 | 0.65 | 0.5 | 0.5 |
| $E_d$ | [MJ/kg] | | | 46 | | |
| $\rho_{hyd}$ | [kg/m$^3$] | | | 920 | | |
| β | [--] | 2.5 | 1.35 | 2.7 | 1.4 | 1.2 |
| e | [--] | 0.88 | 0.63 | 0.89 | 0.66 | 0.49 |
| RE | [MJ/m$^3$] * | 1703.7 | 3034.8 | 3210.5 | 2274.3 | 1184.3 |
| Price (**) | [USD/MJ] | | 4220 | | 16563.5 | 16510.75 |

(*) MJ per volume of dissociated gas

(**) Data from www.ferc.gov, 2013

## 5 Comparison with Literature

Numerical simulations show the time evolution of gas production typically for several years. However, the analysis conducted here is for steady state conditions at the end of gas production. Table 5 shows input values and numerical simulations results. Figure 8 compares numerical and analytical results. The close-form analytical solutions presented here predicts ultimate radius of dissociation to be within 1 and 1.15 the numerically computed value. The difference may be due to the fact that none of the numerical simulations are run to the ultimate radius, but a radius close to the final value.

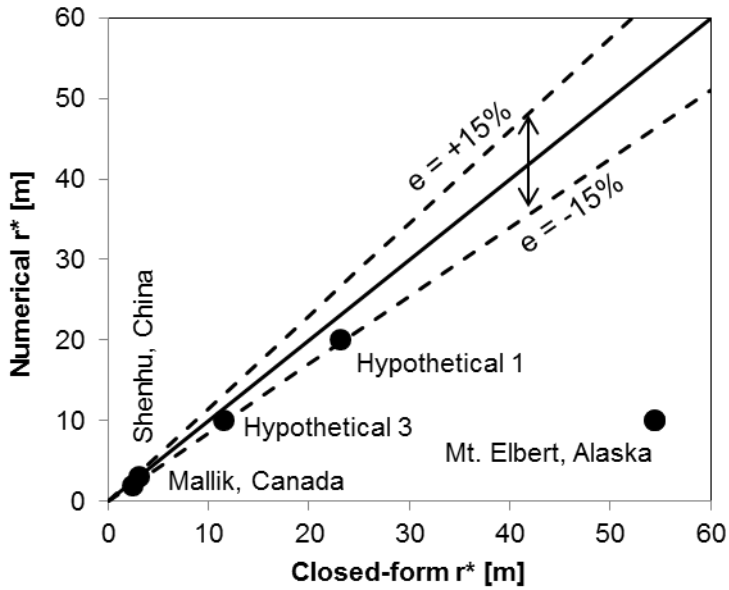


**Figure 8.** Comparison with literature cases. Dissociation front computed tends to be larger than the values from the literature but contained in a 15% error area. Note that Mt. Elbert simulations were stopped after 10800 days of production, therefore no ultimate radius of dissociation was reached.

Table 5: Data input for equations for selected cases

| Case | H [m] | $r_w$ [m] | b (*) [m] | $k_{sed}$ [m/s] | $k_{hbs}$ [m/s] | k' [m/s] | $S_{hyd}$ [--] | $h_w$ [MPa] | $h_{far}$ [MPa] | h* (**) [MPa] | Data based on: | Solution r* [m] | Solution Vol gas [m3] |
|---|---|---|---|---|---|---|---|---|---|---|---|---|---|
| Hypothetical 1 | 1 | 0.1 | 1 | $6.5\ 10^{-9}$ | $3.810^{-9}$ | $1.010^{-14}$ | 0.10 | 2.70 | 5.70 | 4.70 | Moridis et al (2007) | **23.1** | $1.210^{4}$ |
| Hypothetical 2 | 15 | 0.1 | 1 | $6.5\ 10^{-6}$ | $1.910^{-9}$ | $1.010^{-14}$ | 0.70 | 3.00 | 12.00 | 11.20 | Moridis et al (2006) | **3750.0** | $2.510^{10}$ |
| Hypothetical 3 | 50 | 0.1 | 1 | $3.2\ 10^{-6}$ | $5.110^{-7}$ | $3.010^{-6}$ | 0.60 | 4.00 | 12.00 | 11.80 | Konno et al (2010) | **11.5** | $9.110^{5}$ |
| Mallik, Canada | 20 | 0.1 | 1 | $1.310^{-7}$ | $2.110^{-9}$ | $1.010^{-7}$ | 0.50 | 3.00 | 11.00 | 9.40 | Moridis et al (2004) | **2.5** | 1.05E+04 |
| Mt Elbert, Alaska | 11.3 | 0.1 | 1 | $6.510^{-6}$ | $5.7\ 10^{-9}$ | $1.010^{-10}$ | 0.65 | 3.00 | 6.40 | 3.20 | Moridis et al (2011) | **54.4** | $5.0\ 10^{6}$ |
| Shenhu, China | 10 | 0.1 | 1 | $6.510^{-8}$ | $3.910^{-9}$ | $1.010^{-7}$ | 0.30 | 3.00 | 12.00 | 11.84 | Su et al (2012) | **3.2** | $6.910^{3}$ |
| Ulleung Basin, Korea | 70 | 0.1 | 1 | $3.210^{-6}$ | $2.210^{-9}$ | $1.010^{-12}$ | 0.70 | 3.00 | 23.00 | 11.60 | Moridis et al (2013) | **1600.0** | $3.8\ 10^{10}$ |
| Nankai Trough, Japan | 22 | 0.1 | 1 | $6.510^{-7}$ | $1.310^{-8}$ | $1.010^{-12}$ | 0.50 | 3.00 | 13.00 | 11.60 | Kurihara et al (2009) | **1700.0** | $7.510^{9}$ |

(*) Assumed values

(**) Computed from temperature following Kwon et al (2008)

(***) Obtained from hydrate saturation front figures

H = hydrate bearing sediment layer thickness; r* = radius of dissociation; $r_w$ = radius of the well; b = aquitard thickness; $k_{sed}$ = sediment hydraulic conductivity; $k_{hbs}$ = hydrate bearing sediment hydraulic conductivity; k' = aquitard hydraulic conductivity; $S_{hyd}$ = hydrate saturation; $h_w$ = well pressure; $h_{far}$ = far field pressure, h* = dissociation pressure

ND = no data provided

Table 5: Data input for equations for selected cases (cont.)

| | Solutions from numerical simulations | | | |
|---|---|---|---|---|
| **Case** | **r* (***) [m]** | **Vol gas [m3]** | **Observations** | **Reference** |
| Hypothetical 1 | **20.0** | $5\ 10^{3}$ | Confined aquifer | Moridis et al (2007) |
| Hypothetical 2 | **ND** | $1\ 10^{8}$ | Class 1 reservoir: free gas zone - Confined aquifer | Moridis et al (2006) |
| Hypothetical 3 | **10.0** | $1\ 10^{8}$ | Class 3 reservoir - non confined aquifer | Konno et al (2010) |
| Mallik, Canada | **2.0** | ND | | Moridis et al (2004) |
| Mt Elbert, Alaska | **10.0** | $5.5\ 10^{6}$ | Simulation stopped after 10800 production days (not ultimate radious) | Moridis et al (2011) |
| Shenhu, China | **4.0** | $9\ 10^{3}$ | | Su et al (2012) |
| Ulleung Basin, Korea | **250.0** | $9\ 10^{7}$ | r* reaches the boundary of the simulations - Confined aquifer | Moridis et al (2013) |
| Nankai Trough, Japan | **120.0** | $3\ 10^{7}$ | r* reaches the boundary of the simulations - Confined aquifer | Kurihara et al (2009) |

(*) Assumed values
(**) Computed from temperature following Kwon et al (2008)
(***) Obtained from hydrate saturation front figures
ND = no data provided

## 6 Discussion: Real Case Scenario

The decrease in pore water pressure causes an increase in effective stress, volume compaction and the decreased sediment permeability $k_{sed}$. This is demonstrated next for the case of radial flow. Water pressure distribution is (Muskat 1946):

$$u(r) = \frac{h_{far} - h_w}{log\left(r_{far}/r_w\right)} log\left(\frac{r}{r_w}\right) + h_w \tag{32}$$

Effective stress is a function of the initial total stress $\sigma_o$ at the depth of the reservoir. The change in void ratio for large stress is estimated as ($e_{1kPa}$ is the void ratio at σ' = 1 kPa and β a soil parameter):

$$e(\sigma') = e_{1MPa}\left(\frac{\sigma'}{1MPa}\right)^{-\beta} \tag{33}$$

Where $e_{1kPa}$ is an arbitrary reference value of void ratio; β a soil parameter.

Permeability can be found from (Ren and Santamarina; $k_{1kPa}$ is the reference permeability at σ' = 1 kPa and b is a soil parameter which depends on specific surface – for the case of coarse grained soils b = 3.5):

$$k(e) = k_{1MPa}\left(\frac{e}{e_{1MPa}}\right)^{b} \tag{34}$$

With this new change in permeabilities, the pore water pressure distribution will be modified again. Note that the new pore water pressure distribution will lead a change in effective stress, void ratio and permeability. Figure 9 shows an example for the data from Nankai Trough (summarized in Table 6). Figure 9-a represents the initial pore pressure and effective stress distribution on the well and its impact on the void ratio, hydraulic conductivity and flow rate for a steady state condition (Figure 9-b, –c and –d). The permeability and flow rate fall several orders of magnitude.

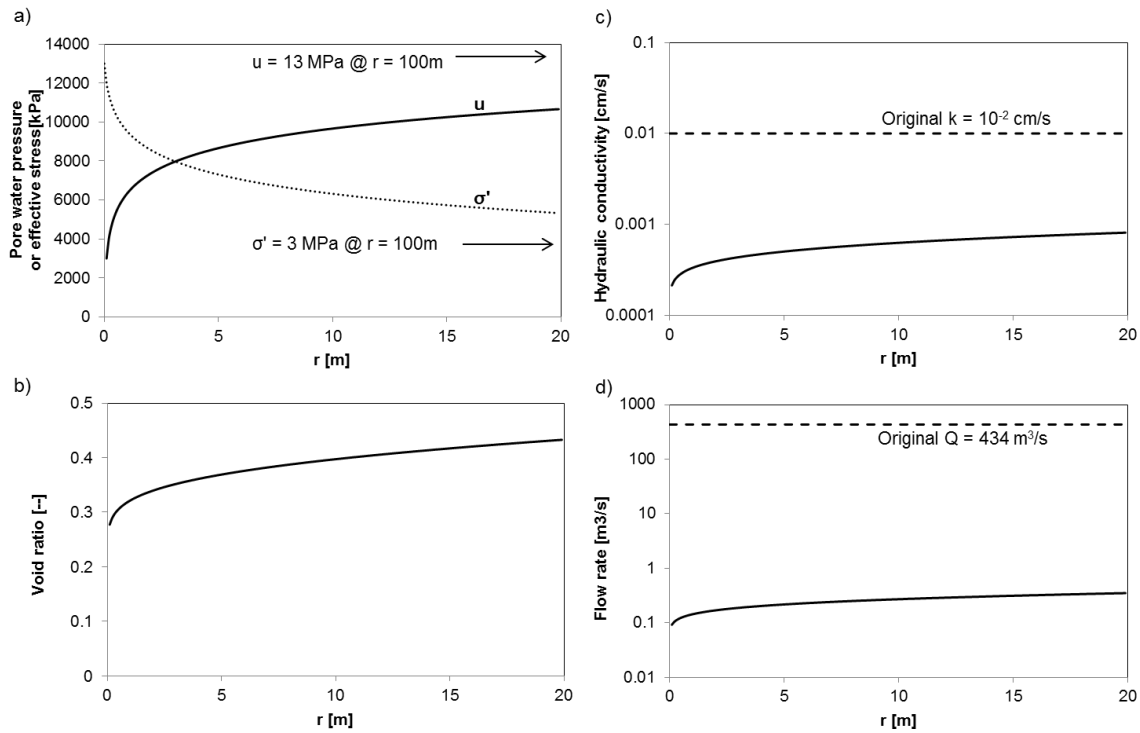


**Figure 9.** Example of gas hydrate production from a marine environment under depressurization strategy (Summary of parameters used can be found in Table 6).

Table 6: Summary of parameters for the example in Figure 9

| Parameter | Symbol | Units | Value |
|---|---|---|---|
| Total stress in the reservoir | $\sigma$ | [kPa] | 16000 |
| Initial water pressure | $h_{far}$ | [kPa] | 13000 |
| Well water pressure | $h_w$ | [kPa] | 3000 |
| Radius of influence | $r_{far}$ | [m] | 100 |
| Radius of the well | $r_w$ | [m] | 0.1 |
| Reservoir thickness | H | [m] | 1 |
| Permeability exponent | b | [--] | 3.5 |
| Void ratio exponent | $\beta$ | [--] | 0.5 |
| Reference void ratio | $e_{1MPa}$ | [--] | 1 |
| Reference permeability | $k_{1MPa}$ | [cm/s] | $10^{-2}$ |

## 7 Conclusions

- Gas production by depressurization is limited by the size of the zone that can be taken outside the stability field. Two cases are analyzed: homogeneous spherical flow

conditions and layered leaky aquifer. Close form solutions predict the size of the affected zone within 15% values estimated with complex numerical simulators.

- The analytical solutions show the interplay between the variables: relative sediment permeabilities $k_{sed}/k_{hbs}$, the leakage in the aquifer $k'/k_{sed}$, relative pressure dissociation $(h^* - h_w)/(h_{far} - h^*)$ and a geometrical ratio $H\ b/r_w^2$.
- Results reflect the complexity of gas recovery from deep sediments included limited affected zone, large changes in effective stress and associated reductions in permeability.

**References**


Anderson, B. J., Wilder, J. W., Kurihara, M., White, M. D., Moridis, G. J., Wilson, S. J., Pooladi-Darvish, M., Masuda, Y., Collett, T. S., and Hunter, R. (2008). "Analysis of modular dynamic formation test results from the Mount Elbert 01 stratigraphic test well, Milne Point Unit, North Slope, Alaska." 6th International Conference on Gas Hydrates (ICGH 2008)Vancouver, British Columbia, Canada.

Boswell, R., and Collett, T. S. (2011). "Current perspectives on gas hydrate resources." Energy & Environmental Science, 4(4), 1206-1215.

Dallimore, S. R., Wright, J. F., Nixon, F. M., Kurihara, M., Yamamoto, K., Fujii, T., Fujii, K., Numasawa, M., Yasuda, M., and Imasato, Y. "Geologic and porous media factors affecting the 2007 production response characteristics of the JOGMEC/NRCAN/AURORA Mallik Gas Hydrate Production Research Well." Proc., Proceedings of the 6th International Conference on Gas Hydrates (ICGH 2008), 10.

De Glee, G. (1951). "Berekeningsmethoden voor de winning van grondwater." Drinkwatervoorziening, 3e Vacantiecursus, 38-80.

Esmaeilzadeh, F., Zeighami, M. E., and Kaljahi, J. F. (2011). "1-D Mathematical Modeling of Hydrate Decomposition in Porous Media by Depressurization and Thermal Stimulation." Journal of Porous Media, 14(1).

Fujii, T., Saeki, T., Kobayashi, T., Inamori, T., Hayashi, M., Takano, O., Takayama, T., Kawasaki, T., Nagakubo, S., and Nakamizu, M. (2013) "Resource assessment of methane hydrate in the Eastern Nankai Trough Japan." Proc., 6th International Conference on Gas Hydrates (ICGH 2008), 68.

Goel, N., Wiggins, M., and Shah, S. (2001). "Analytical modeling of gas recovery from in situ hydrates dissociation." Journal of Petroleum Science and Engineering, 29(2), 115-127.

Guide, C.-S. U. s. (2012). "Computer Modeling Group Ltd."

Hancock, S., Collett, T., Dallimore, S., Satoh, T., Inoue, T., Huenges, E., Henninges, J., and Weatherill, B. (2005). "Overview of thermal-stimulation production-test results for the JAPEX/JNOC/GSC et al. Mallik 5L-38 gas hydrate production research well." Geological Survey of Canada, 135.

Hermann, W. A. (2006). "Quantifying global exergy resources." Energy, 31(12), 1685-1702.

Hong, H., and Pooladi-Darvish, M. (2005). "Simulation of depressurization for gas production from gas hydrate reservoirs." Journal of Canadian Petroleum Technology, 44(11), 39-46.

Hong, H., Pooladi-Darvish, M., and Bishnoi, P. (2003). "Analytical modelling of gas production from hydrates in porous media." Journal of Canadian Petroleum Technology, 42(11), 45-56.

Jang, J., and Santamarina, J. C. (2011). "Recoverable gas from hydrate- bearing sediments: Pore network model simulation and macroscale analyses." Journal of Geophysical Research: Solid Earth, 116(B8).

Ji, C., Ahmadi, G., and Smith, D. H. (2001). "Natural gas production from hydrate decomposition by depressurization." Chemical Engineering Science, 56(20), 5801-5814.

Klar, A., Uchida, S., Soga, K., and Yamamoto, K. (2013). "Explicitly coupled thermal flow mechanical formulation for gas-hydrate sediments." SPE Journal, 18(02), 196-206.

Konno, Y., Masuda, Y., Hariguchi, Y., Kurihara, M., and Ouchi, H. (2010). "Key factors for depressurization-induced gas production from oceanic methane hydrates." Energy & Fuels, 24(3), 1736-1744.

Kurihara, M., Sato, A., Ouchi, H., Narita, H., Masuda, Y., Saeki, T., and Fujii, T. (2009). "Prediction of gas productivity from Eastern Nankai Trough methane-hydrate reservoirs." SPE Reservoir Evaluation & Engineering, 12(03), 477-499.

Kwon, T. H., Cho, G. C., and Santamarina, J. C. (2008). "Gas hydrate dissociation in sediments: Pressure- temperature evolution." Geochemistry, Geophysics, Geosystems, 9(3).

Li, G., Moridis, G. J., Zhang, K., and Li, X.-S. (2010). "Evaluation of gas production potential from marine gas hydrate deposits in Shenhu area of South China Sea." Energy & Fuels, 24(11), 6018-6033.

Li, X.-S., Yang, B., Li, G., and Li, B. (2012). "Numerical simulation of gas production from natural gas hydrate using a single horizontal well by depressurization in Qilian Mountain permafrost." Industrial & Engineering Chemistry Research, 51(11), 4424-4432.

Moridis, G., and Collett, T. (2003). "Strategies for gas production from hydrate accumulations under various geologic conditions." Lawrence Berkeley National Laboratory, Lawrence Berkeley National Laboratory, Berkeley, CA.

Moridis, G. J. (2014). "TOUGH+ HYDRATE v1. 2 User's Manual: A Code for the Simulation of System Behavior in Hydrate-Bearing Geologic Media." R. LBNL-3185, ed., Lawrence Berkeley National Laboratory, Berkeley, CA.

Moridis, G. J., Collett, T., Boswell, R., Kurihara, M., Reagan, M. T., Koh, C., and Sloan Jr, E. D. (2008). "Toward production from gas hydrates: current status, assessment of resources, and simulation-based evaluation of technology and potential." SPE 114163, Keystone, Colo.

Moridis, G. J., Collett, T., Pooladi-Darvish, M., Hancock, S., Santamarina, J. C., Boswell, R., Kneafsey, T. J., Rutqvist, J., Kowalsky, M. B., Reagan, M. T., Sloan Jr, E. D., Sum, A. K., and Koh, C. (2011). "Challenges, uncertainties and issues facing gas production from gas hydrate deposits." SPE Reservoir Evaluation & Engineering, 14(1), 76-112.

Moridis, G. J., Collett, T. S., Dallimore, S. R., Satoh, T., Hancock, S., and Weatherhill, B. (2002). "Numerical simulation studies of gas production scenarios from hydrate accumulations at the Mallik Site, McKenzie Delta, Canada." 4th Int.Conf. Gas Hydrates, 239-244.

Moridis, G. J., Kim, J., Reagan, M. T., and Kim, S.-J. (2013). "Feasibility of gas production from a gas hydrate accumulation at the UBGH2-6 site of the Ulleung basin in the Korean East Sea." Journal of Petroleum Science and Engineering, 108, 180-210.

Moridis, G. J., Kowalsky, M. B., and Pruess, K. (2007). "Depressurization-induced gas production from class-1 hydrate deposits." SPE Reservoir Evaluation & Engineering, 10(5), 458-481.

Moridis, G. J., and Sloan, E. D. (2007). "Gas production potential of disperse low-saturation hydrate accumulations in oceanic sediments." Energy Conversion and Management, 48(6), 1834-1849.

Muskat, M. (1965). Flow of homogeneous fluids. JW Edwards, J.W. Edwards Inc., Ann Arbor, Michigan.

Myshakin, E. M., Gaddipati, M., Rose, K., and Anderson, B. J. (2012). "Numerical simulations of depressurization-induced gas production from gas hydrate reservoirs at the Walker Ridge 313 site, northern Gulf of Mexico." Marine and Petroleum Geology, 34(1), 169-185.

Pooladi-Darvish, M. (2004). "Gas production from hydrate reservoirs and its modeling." Journal of Petroleum Technology, 56(6), 65-71.

Santamarina, J., and Jang, J. (2009). "Gas production from hydrate bearing sediments: geomechanical implications." DOE-NETL Fire in the Ice, 9(4), 18-22.

Shankar, U., and Riedel, M. (2011). "Gas hydrate saturation in the Krishna–Godavari basin from P-wave velocity and electrical resistivity logs." Marine and Petroleum Geology, 28(10), 1768-1778.

Sloan Jr, E. D., and Koh, C. (2007). Clathrate hydrates of natural gases, Marcel Dekker, New York.

Stone, H. (1970). "Probability model for estimating three-phase relative permeability." Journal of Petroleum Technology, 22(02), 214-218.

Su, Z., He, Y., Wu, N., Zhang, K., and Moridis, G. J. (2012). "Evaluation on gas production potential from laminar hydrate deposits in Shenhu Area of South China Sea through depressurization using vertical wells." Journal of Petroleum Science and Engineering, 86, 87-98.

Tsypkin, G. G. (2000). "Mathematical models of gas hydrates dissociation in porous media." Annals of the New York Academy of Sciences, 912(1), 428-436.

Ullerich, J., Selim, M., and Sloan, E. (1987). "Theory and measurement of hydrate dissociation." AIChE Journal, 33(5), 747-752.

Walsh, M. R., Hancock, S. H., Wilson, S. J., Patil, S. L., Moridis, G. J., Boswell, R., Collett, T. S., Koh, C. A., and Sloan, E. D. (2009). "Preliminary report on the commercial viability of gas production from natural gas hydrates." Energy Economics, 31(5), 815-823.

Wu, N., Yang, S., Zhang, H., Liang, J., Wang, H., and Lu, J. a. (2010) "Gas Hydrate System of Shenhu Area Northern South China Sea: Wire-line Logging Geochemical Results and Preliminary Resources Estimates." Paper 20485. Proc., Offshore Technology Conference.

Yamamoto, K., and Dallimore, S. (2008). "Aurora-JOGMEC-NRCan Mallik 2006-2008 gas hydrate research project progress." Natural Gas & Oil, 304, 285-4541.

## PRODUCTS

**Publications – Presentations:**

- A session on "Hydrate bearing soils: characterization, modeling and geomechanical implications", was organized for the forthcoming AGU Fall meeting 2015, San Francisco, 15th to 19th December 2014. Marcelo Sanchez is one of the session conveners.
- Carlos Santamarina was invited to deliver an invited lecture on hydrate bearing Sediments at the AGU Fall meeting 2015.
- A conference paper has been accepted at the XVI ECSMGE 2015. Edinburgh, UK, September 13-17 2015 Title: "Numerical Modeling of Gas Hydrate Bearing Sediments". Authors: M. Sanchez, J. C. Santamarina. A. Shastri & Xuerui Gai.

**Website:** Publications (for academic purposes only) and key presentations are included in http://pmrl.ce.gatech.edu/; http://ceprofs.civil.tamu.edu/msanchez/

**Technologies or techniques:** None at this point.

**Inventions, patent applications, and/or licenses:** None at this point.

**Other products:** None at this point.

## PARTICIPANTS

*Research Team*: The current team is shown next.

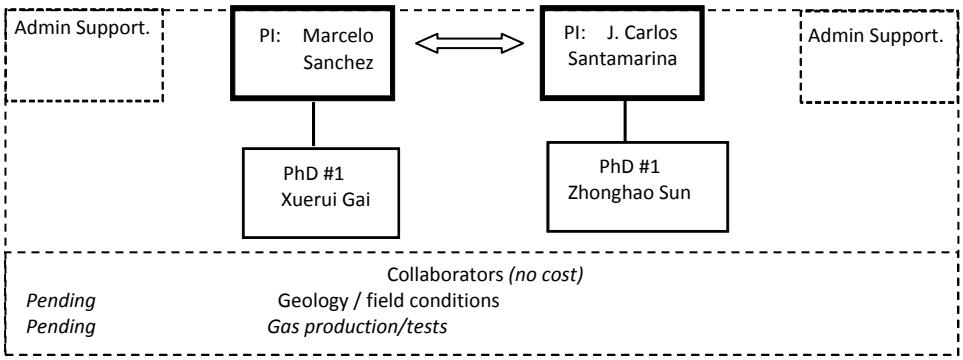


## IMPACT

- While it is still too early to assess impact, we can already highlight the computational platform extensively validated in a wide range of coupled thermo-hydro-chemo-mechanical coupled problems (CB_Hydrate).

## CHANGES/PROBLEMS:

None so far.

## SPECIAL REPORTING REQUIREMENTS:

Nothing to report

# BUDGETARY INFORMATION:

## TAMU

| | | | | | | | | | | | | | | | | |
|---|---|---|---|---|---|---|---|---|---|---|---|---|---|---|---|---|
| | | | | Budget Period 1 | | | | | | | | Budget Period 2 | | | | |
| | Q1 | | Q2 | | Q3 | | Q4 | | Q1 | | Q2 | | Q3 | | Q4 | |
| | Enter date range | | Enter date range | | Enter date range | | Enter date range | | Enter date range | | Enter date range | | Enter date range | | Enter date range | |
| Baseline Reporting Quarter | 10/1/13-12/31/13 | | 01/01/14-03/31/14 | | 04/01/14-06/30/14 | | 07/01/14-9/30/14 | | 10/1/14-12/31/2014 | | 01/01/15-03/31/15 | | 04/01/15-06/30/15 | | 07/01/15-9/30/15 | |
| | | Cumulative | | Cumulative | | Cumulative | | Cumulative | | Cumulative | | Cumulative | | Cumulative | | Cumulative |
| | Q1 | Total | Q2 | Total | Q3 | Total | Q4 | Total | Q1 | Total | Q2 | Total | Q3 | Total | Q4 | Total |
| **Baseline Cost Plan** | $ 30,300.00 | $30,300.00 | $30,300.00 | $60,600.00 | $ 30,300.00 | $ 90,900.00 | $ 88,667.00 | $179,567.00 | $ 40,000.00 | $219,567.00 | | | | | | |
| Federal Share | $ 30,300.00 | $30,300.00 | $30,300.00 | $60,600.00 | $ 30,300.00 | $ 90,900.00 | $ 88,667.00 | $179,567.00 | $ 40,000.00 | $219,567.00 | | | | | | |
| Non-Federal Share | $ 11,223.00 | $11,223.00 | $11,223.00 | $22,446.00 | $ 11,223.00 | $ 33,669.00 | $ 11,223.00 | $ 44,892.00 | $ 11,223.00 | $ 56,115.00 | | | | | | |
| Total Planned | $ 41,523.00 | $41,523.00 | $41,523.00 | $83,046.00 | $ 41,523.00 | $124,569.00 | $ 99,890.00 | $224,459.00 | $ 51,223.00 | $275,682.00 | | | | | | |
| **Actual Incurred Costs** | $ 5,301.83 | $ 5,301.83 | $13,764.34 | $19,066.17 | $ 33,827.48 | $ 52,893.65 | $ 51,567.77 | $104,461.42 | $ 80,352.17 | $184,813.59 | | | | | | |
| Federal Share | $ 3,335.02 | $ 3,335.02 | $ 9,848.68 | $13,183.70 | $ 10,170.37 | $ 23,354.07 | $ 58,205.62 | $ 81,559.69 | $ 92,208.79 | $173,768.48 | | | | | | |
| Non-Federal Share | $ 5,182.96 | $ 5,182.96 | $20,751.77 | $25,934.73 | $ 20,743.19 | $ 46,677.92 | $ 29,262.19 | $ 75,940.11 | $ - | $ 75,940.11 | | | | | | |
| Total Incurred costs | $ 8,517.98 | $ 8,517.98 | $30,600.45 | $39,118.43 | $ 30,913.56 | $ 70,031.99 | $ 87,467.81 | $157,499.80 | $ 92,208.79 | $249,708.59 | | | | | | |
| **Varience** | $ 33,005.02 | $33,005.02 | $10,922.55 | $43,927.57 | $ 10,609.44 | $ 54,537.01 | $ 12,422.19 | $ 66,959.20 | $(40,985.79) | $ 25,973.41 | | | | | | |
| Federal Share | $ 1,966.81 | $ 1,966.81 | $ 3,915.66 | $ 5,882.47 | $ 23,657.11 | $ 29,539.58 | $ (6,637.85) | $ 22,901.73 | $ 11,045.11 | $ 11,045.11 | | | | | | |
| Non-Federal Share | $ 6,040.04 | $ 6,040.04 | $ (9,528.77) | $ (3,488.73) | $ (9,520.19) | $ (13,008.92) | $(40,485.19) | $ (53,494.11) | $ 11,223.00 | $ 11,223.00 | | | | | | |
| **Total Varience** | $ 8,006.85 | $ 8,006.85 | $ (5,613.11) | $ 2,393.74 | $ 14,136.92 | $ 16,530.66 | $(47,123.04) | $ (30,592.38) | $ 22,268.11 | $ 22,268.11 | | | | | | |

## GT

| | | | | | | | | | | | | | | | | |
|---|---|---|---|---|---|---|---|---|---|---|---|---|---|---|---|---|
| | Budget Period 1 | | | | | | | | Budget Period 2 | | | | | | | |
| | Q1 | | Q2 | | Q3 | | Q4 | | Q1 | | Q2 | | Q3 | | Q4 | |
| **Baseline Reporting Quarter DE-FE0013889** | 10/1/13 - 12/31/13 | | 1/1/14 - 3/31/14 | | 4/1/14 - 6/30/14 | | 7/1/14 - 9/30/14 | | 10/1/14 - 12/31/14 | | 1/1/15 - 3/31/15 | | 4/1/15 - 6/30/15 | | 7/1/15 - 9/30/15 | |
| | Q1 | Cumulative Total | Q2 | Cumulative Total | Q3 | Cumulative Total | Q4 | Cumulative Total | Q1 | Cumulative Total | Q2 | Cumulative Total | Q3 | Cumulative Total | Q4 | Cumulative Total |
| **Baseline Cost Plan** | | | | | | | | | | | | | | | | |
| Federal Share | 21,556 | 21,556 | 21,556 | 43,112 | 21,556 | 64,667 | 21,556 | 86,223 | 18,000 | 104,223 | 18,000 | 122,223 | 18,000 | 140,223 | 34,658 | 174,881 |
| Non-Federal Share | 7,315 | 7,315 | 7,315 | 14,630 | 7,316 | 21,946 | 7,316 | 29,262 | 7,535 | 36,797 | 7,535 | 44,332 | 7,535 | 51,866 | 14,100 | 65,966 |
| Total Planned | 28,871 | 28,871 | 28,871 | 57,742 | 28,872 | 86,613 | 28,872 | 115,485 | 25,535 | 141,020 | 25,535 | 166,555 | 25,535 | 192,089 | 48,758 | 240,847 |
| **Actual Incurred Cost** | | | | | | | | | | | | | | | | |
| Federal Share | 0 | 0 | 11,228 | 11,228 | 11,458 | 22,685 | 48,488 | 71,174 | 21,192 | 92,366 | | | | | | |
| Non-Federal Share | 0 | 0 | 0 | 0 | 21,946 | 21,946 | -20 | 21,926 | 16,170 | 38,096 | | | | | | |
| Total Incurred Costs | 0 | 0 | 11,228 | 11,228 | 33,404 | 44,631 | 48,468 | 93,099 | 37,362 | 130,461 | | | | | | |
| **Variance** | | | | | | | | | | | | | | | | |
| Federal Share | -21,556 | -21,556 | -10,328 | -31,884 | -10,098 | -41,982 | 26,933 | -15,049 | 3,192 | -11,857 | | | | | | |
| Non-Federal Share | -7,315 | -7,315 | -7,315 | -14,630 | 14,630 | 0 | -7,336 | -7,336 | 8,635 | 1,299 | | | | | | |
| Total Variance | -28,871 | -28,871 | -17,643 | -46,514 | 4,532 | -41,982 | 19,596 | -22,386 | 11,827 | -10,559 | | | | | | |

**National Energy Technology Laboratory**

626 Cochrans Mill Road
P.O. Box 10940
Pittsburgh, PA 15236-0940

3610 Collins Ferry Road
P.O. Box 880
Morgantown, WV 26507-0880

13131 Dairy Ashford Road, Suite 225
Sugar Land, TX 77478

1450 Queen Avenue SW
Albany, OR 97321-2198

Arctic Energy Office
420 L Street, Suite 305
Anchorage, AK 99501

Visit the NETL website at:
www.netl.doe.gov

Customer Service Line:
1-800-553-7681